Journal of Adhesion Science and Technology

ISSN: 0169-4243 (Print) 1568-5616 (Online) Journal homepage: http://www.tandfonline.com/loi/tast20

Experimental study on bond behavior between corrosion-cracked reinforced concrete and CFRP sheets

Rami H. Haddad & Abeer A. Al Dalou

To cite this article: Rami H. Haddad & Abeer A. Al Dalou (2017): Experimental study on bond behavior between corrosion-cracked reinforced concrete and CFRP sheets, Journal of Adhesion Science and Technology, DOI: 10.1080/01694243.2017.1371912

To link to this article: http://dx.doi.org/10.1080/01694243.2017.1371912

JOURNAL OF ADHESION SCIENCE AND TECHNOLOGY, 2017
https://doi.org/10.1080/01694243.2017.1371912

Taylor & Francis
Taylor & Francis Group

Experimental study on bond behavior between corrosion-cracked reinforced concrete and CFRP sheets

Rami H. Haddad[a] and Abeer A. Al Dalou[b]

[a]Department of Civil Engineering, Jordan University of Science and Technology, Irbid, Jordan; [b]Department of Civil Engineering, Al-Ahliyya Amman University, Amman, Jordan

ABSTRACT

Bond behavior between corrosion damaged reinforced concrete and carbon fiber reinforced concrete polymer (CFRP) sheets was experimentally investigated. Forty ordinary strength concrete blocks (150 × 150 × 200 mm) were reinforced at one side across the 200-mm-dimension using three conventional ϕ12 mm steel bars at a spacing of (30, 40, and 50 mm) at a concrete clear cover of 15 mm. Thirty blocks were subjected to a cyclic treatment in 3% chloride solution until corrosion initiated and resulted in three different global cracking widths of up to 0.90 mm. Both control and corrosion damaged blocks were attached to CFRP sheets over their steel reinforced zone at bond lengths and widths ranging from (90 to 150 mm) and (50 to 150 mm), respectively, with CFRP bond length-to-bar spacing ratio kept constant at 1/3. Near-end pull-off tests were carried out using a special setup, mounted on a Universal Testing machine. Corrosion cracking caused significant reductions in bond strength, and slippage at ultimate stress at (41 and 68%), respectively. Other bond characteristics such as stress at first slippage, and bond stiffness and toughness were reduced, as well, by as high as (83, 44 and 67%) of those of control specimens, respectively. Corrosion cracks were more detrimental for smaller bond length and width values; especially after first and second corrosion stages, where bond failure was categorized by concrete skin peeling-off.

ARTICLE HISTORY
Received 3 February 2017
Revised 21 August 2017
Accepted 22 August 2017

KEYWORDS
Corrosion cracks; bond failure; bond characteristics; pull-off specimens

1. General

In field, concrete structures may be subjected to different forms of attack; the most common of which is chloride induced corrosion; especially in coastal environments or whenever deicing agent are used. Once chloride concentration at steel location surpasses a certain threshold value, corrosion initiates and progresses towards cracking of concrete; aggravating the physical states of exposed structural elements [1]. Beams and slabs (or bridge decks) are the most susceptible because their horizontal alignment allow easy intrusion of chloride and hence corrosion initiation and progression. Corrosion damage accompanied with loss in reinforcing steel cross-sectional area as well as undesirable changes in steel surface

CONTACT Rami H. Haddad rhaddad@just.edu.jo

characteristics and mechanical properties result in sever reductions in the mechanical performance of flexural members [2–6]. Thus, repair becomes essential to preserve structural integrity and prevent catastrophic failures; especially in bridge decks.

Repair of corroded flexural elements goes through several steps represented in removal of concrete cover, cleaning of rust, protecting steel, replacing concrete cover with new one, and finally providing additional reinforcement using either concrete jackets, steel plates, or fiber reinforced polymer composites (FRP) [7–10]. Even if existing concrete cover in corroded elements is replaced as a standard measure before strengthening, the probability of cracks' reappearance in newly cast concrete cover remains high. As well stipulated, cracking of concrete cover in beams or slabs impact negatively their bond with carbon fiber reinforced polymer (CFRP), attached to regain flexural load capacity; undermining the significance of the proposed repair process [11–13].

The intensity, distribution, and size of cracking are key factors that determine the degradation extent in bond between damaged concrete and attached FRP composites [11–14]. Presence of openings in concrete structural elements was stipulated to impact negatively their performance unless efficient repair techniques were applied [15]. Recent published works indicated that cracks, produced by heating of concrete to temperatures of 600 °C, had resulted in significant degradation in bond strength between heat-damaged concrete and CFRP sheets reaching as high 64% [11,12]. Pre and post-repair sodium sulfate attack on flexural elements had a less negative impact on bond behavior between concrete and attached CFRP sheets represented in loss of bond strength by as much as 40% [13]. Load induced cracks are wider yet are more localized than durability induced ones; hence their effect on bond behavior would be different [14]. Thermal incompatibility between FRP and concrete induces additional concrete cover cracking hence aggravates bond performance further [16].

2. Problem statement, objectives and scope

Fiber reinforced polymer (FRP) composites have been used on a large scale in repairing various structural steel and reinforced concrete elements. Yet, the use of such a technique in repairing flexural elements with corroding steel reinforcement is still questionable because of the negative impact of corrosion induced cracks upon bond characteristics between concrete and the FRP composites. Until now, the extent of degradation in bond characteristics between FRP and concrete having pre-existing corrosion cracking has not been well established, and requires further investigation. In present work, the effect of cracks resulting from steel corrosion in concrete two slabs on the bond with attached CFRP sheets is evaluated considering corrosion cracks' size, as well as CFRP sheets' bond length and width. Cracks perpendicular to the fibers of externally attached CFRP sheets are studied in the present; simulating cracked repaired slabs.

Forty ordinary concrete strength blocks (150 × 150 × 200) with reinforcing steel, embedded along the 200-mm-dimension at spacing values of 30, 40 and 50 mm, were cast then cured for 28-days strength. Afterwards, thirty reinforced concrete blocks were subjected to a special treatment in a chloride solution for periods from 60 to 120 days to generate corrosion cracks at global widths; ranging from 0.18 to 0.90 mm. The remaining ten concrete blocks were left for similar periods in lime water, as controls. Finally, CFRP sheets of varying bond lengths (90, 120, and 150 mm) and widths (50, 100, and 150) were attached to these blocks on their cracked side (150 × 200 mm) and the opposite one using a special epoxy. Bond behavior was

later evaluated using a special setup designed to allow de-bonding of the CFRP sheets from the block side where reinforcement was placed while concrete was being subjected to tensile stressing. Obtained experimental data were analyzed for bond behavior and its characteristics. The use of the present modified bond specimen contributed to simplifying corrosion treatment and reducing experimental testing time and effort while simulated to a very good extent bond behavior between cracked concrete flexural members and CFRP sheets. Subramaniam et al. [17] applied similar stress condition on shear type bond specimens to investigate the variation in the local interface fracture properties on shear debonding of CFRP composite from concrete.

3. Testing program

To achieve the objective of the study, near-end pull-off specimens were assembled by attaching CFRP sheets to reinforced ordinary strength concrete blocks (150 × 150 × 200 mm) at bond length of (90, 120, and 150 mm) and bond width of (50, 100, and 150 mm). Ten blocks were kept in lime water with the remaining thirty subjected to wetting in chloride solution then drying for 60, 90, and 120 days using a special treatment chamber to create steel corrosion cracking of varying width magnitudes. Corrosion cracking stages designated as one, two, and three corresponded to measured crack width of: (a) less than 0.25 mm; (b) between 0.50 and 0.64 mm; (c) between 0.70 and 1.1 mm, respectively.

Bond stress vs. slip relationship for control and corrosion damaged pull-off specimens were obtained using a special setup, mounted on a universal testing machine. The experimental results, obtained for control and corrosion damaged specimens, were compared to investigate the effect of corrosion cracks on bond behavior and characteristics. The type and number of specimens and their designation is summarized in Table 1. As shown, a letter-number designation was adopted to define both repair configuration and stage of corrosion cracking. For example, W10-L9-S2 refers to pull-off specimens with CFRP sheets bonded at an area of (100 × 90 mm) to concrete blocks with second stage corrosion cracks.

Table 1. Specimen type and task designation.

	Repair configuration		
Designation	L_F (mm)	W_F (mm)	Specimen number
W10-L9-S0	90	100	2
W10-L12-S0	120	100	2
W10-L18-S0	180	100	2
W5-L12-S0	120	50	2
W15-L12-S0	120	150	2
W10-L9-S_{1-3}	90	100	2 × 3
W10-L12-S_{1-3}	120	100	2 × 3
W10-L18-S_{1-3}	180	100	2 × 3
W5-L12-S_{1-3}	120	50	2 × 3
W15-L12-S_{1-3}	120	150	2 × 3
Total			40

Note: L_F, bond length; and W_F, bond width.

4. Testing procedure

4.1. Ingredients and material properties

4.1.1. Concrete mixture

A concrete mixture was prepared using Type I ordinary Portland cement, coarse aggregate (having a maximum aggregate size of 12.5 mm), and a mixture of fine limestone aggregate and silica sand at 70 and 30%, respectively, before used in casting all concrete blocks and standard cylinders (100 × 200 mm). The physical properties of the aggregate particles used were obtained according to ASTM methods C33, C127, C128, and C136 and are listed in Table 2 [18]. The concrete mixture, used in casting various specimens, was proportioned at a w/c ratio of 0.54 according to ACI mix design procedure [19]. The proportions of water, cement, coarse aggregate, fine aggregates, and silica sand were 210, 370, 846, 580, and 249, respectively.

4.1.2. Reinforcing steel

All blocks were reinforced with 3ϕ12 mm steel bars along their 200-mm-long side, as shown in Figure 1. The ratio of spacing between steel bars (S) to the bond length of attached CFRP sheets was kept constant at 1/3. Steel bars were spaced at values of 30, 40, and 50 mm; corresponding to bond lengths of 90, 120, and 150 mm, respectively. The mechanical properties of the reinforcing steel bars, as determined experimentally, are listed in Table 3.

Table 2. Physical properties of mineral aggregates.

	Aggregate type		
Properties	Coarse	Fine	Silica
$BSG_{(SSD)}$	2.56	2.63	2.59
Absorption (%)	2	1.30	0.80
Fineness modulus	NA	3.0	1.70
Unit weight (kg/m^3)	1499	NA	NA

Note: BSG, Bulk Specific Gravity; SSD, Saturated Surface Dry; NA, not applicable.

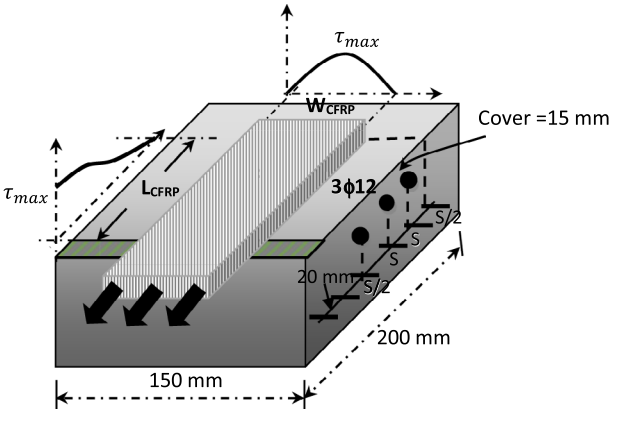

Figure 1. Geomtric confiuration of pull-off specimens including reinforcing steel layout, and shearing stress distribution along bond width and length of CFRP sheets [21].

Table 3. Corrosion cracking stages for different concrete blocks.

Specimen designation	CS	Cracking width (mm)			ML (%)	UPV (km/s)	DI_{UPV} (%)
		CW_1	CW_2	ACW			
W10-L9-S0	NA	NA	NA	NA	NA	4.88	NA
W10-L9-S1	1	0.15	0.25	0.20	2.4	4.70	7
W10-L9-S2	2	0.50	0.63	0.57	3.5	4.51	14
W10-L9-S3	3	0.88	0.98	0.93	5.0	4.16	27
W10-L12-S0	NA	NA	NA	NA	NA	4.93	NA
W10-L12-S1	1	0.15	0.15	0.15	2.3	4.50	17
W10-L12-S2	2	0.58	0.6	0.59	4.0	4.29	24
W10-L12-S3	3	1.1	0.80	0.93	6.2	4.09	31
W10-L15-S0	NA	NA	NA	NA	NA	4.95	NA
W10-L15-S1	1	0.18	0.23	0.20	2.5	4.68	11
W10-L15-S2	2	0.61	0.64	0.64	3.7	4.43	20
W10-L15-S3	3	0.88	0.88	0.88	5.4	4.11	31
W5-L12-S0	NA	NA	NA	NA	NA	4.93	NA
W5-L12-S1	1	0.18	0.16	0.17	2.3	4.50	17
W5-L12-S2	2	0.52	0.54	0.53	4.0	4.29	24
W5-L12-S3	3	1.1	0.82	0.96	6.2	4.09	31
W15-L12-S0	NA	NA	NA	NA	NA	4.93	NA
W15-L12-S1	1	0.20	0.13	0.16	2.3	4.50	17
W15-L12-S2	2	0.58	0.59	0.59	4.0	4.29	24
W15-L12-S3	3	0.85	0.85	0.85	6.2	4.09	31

Notes: NA, Not applicable; ACW, Average crack width; UPV, Ultrasonic pulse velocity; CS, Corrosion stage; ML, mass loss percentage; $DI_{UPV,}$ Damage index in terms of UPV.

4.1.3. CFRP sheet system

CFRP sheets from BASF having a thickness of 0.17 mm were cut from 500-mm wide roll of unidirectional-continuous fiber and attached to the surfaces of different concrete blocks. The mechanical properties for the CFRP sheets, as provided by the manufacturer, namely elastic modulus, ultimate tensile strength, and ultimate strain capacity were 230 GPa, 4.9 GPa, and 2.1%, respectively.

4.1.4. Primer adhesives

BASF adhesive, designated as MBrace Saturant, was used for bonding CFRP sheets to concrete. The adhesive mechanical properties (as provided by the manufacture), namely yield strength, ultimate strength (after 7 days of curing), tensile elastic modulus and tensile rupture strain were 54 MPa, 55.2 MPa, 3.034 GPa and 3.5%, respectively.

4.2. Concrete mixing, casting, and curing

The mixing of the different concrete ingredients was carried using a tilting drum mixer of 0.15 m^3 according to ASTM method C31 [18]. A superplasticizer was added to mixing water at 1% (by cement weight), prior the end of the mixing process, to improve workability. As a quality control measure, slump was carried out according to ASTM method C143: it ranged from 30 to 40 mm for the different batches [18]. The specimens were cast in a specially designed 20-mm-thick wooden molds of net internal dimensions of (150 × 150 × 200 mm). Concrete was placed in the molds in two layers and consolidated using a vibrating Table before the final surface was finished smooth by a trowel, covered with wet burlap for 24 h and placed in a water tank to cure for another 27 days. Standard cylinders were also cast, and cured for a total of 28 days then tested according to ASTM method C 39 [18]. The 28-days

compressive strength for present concrete averaged at about 32 MPa with a coefficient of variation of about 5%; based upon 24 cylinder specimens from twelve concrete batches.

4.3. Corrosion accelerating method

After being curing in water for 28 days, thirty concrete blocks were subjected to cycles of immersion in 3% NaCl solution followed by drying using a special conditioning unit to trigger and accelerate steel corrosion of the bars embedded in these blocks, shown in Figure 2. The unit consists of treatment and storage tanks, connected by a two-way pumping system. The treatment tank is equipped with an electronic regulator which allowed maintaining a temperature of (40 °C) during immersion for two days followed by drying for three days. This treatment cycle continued for 60, 120, and 150 days; during which widths measurements of corrosion-generated cracks were periodically carried out using a crack-measuring device. It is important to mention that the exposed ends of the bars were protected against corrosion using a zinc oxide paint.

4.4. Application procedure of CFRP sheets

The surfaces of concrete blocks, where CFRP sheets are attached, were cleaned using a wire brush mounted on an electric drill to remove cement laitance, loose and friable material hence achieve an open profiled textured surface. Dust was then removed using a vacuum cleaner, before the surface were brushed using a volatile liquid to clean the surface and reduce the moisture content.

The installation of CFRP composites on concrete surfaces followed the following steps. Firstly, the desired lengths and widths of CFRP sheets were obtained using a scissor and the zones where the CFRP sheets are to be attached were marked. Secondly, the adhesive for bonding the CFRP strips were prepared by mixing their two components (A and B) according to the instructions by the manufacturer. Thirdly, the adhesive is applied first at 1.00 kg/m^2 to marked zones, before the sheets were installed and rolled over to become saturated with the resin. Then, another layer of the adhesive at 0.50 kg/m^2 was painted on the

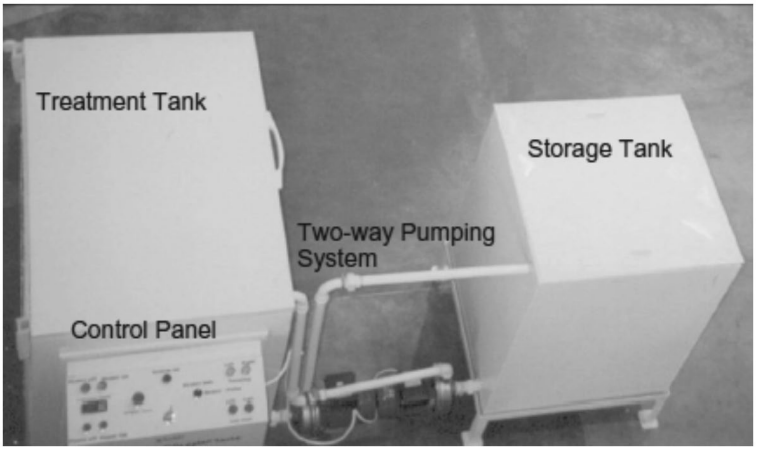

Figure 2. The treatment unit used to accelerate corrosion.

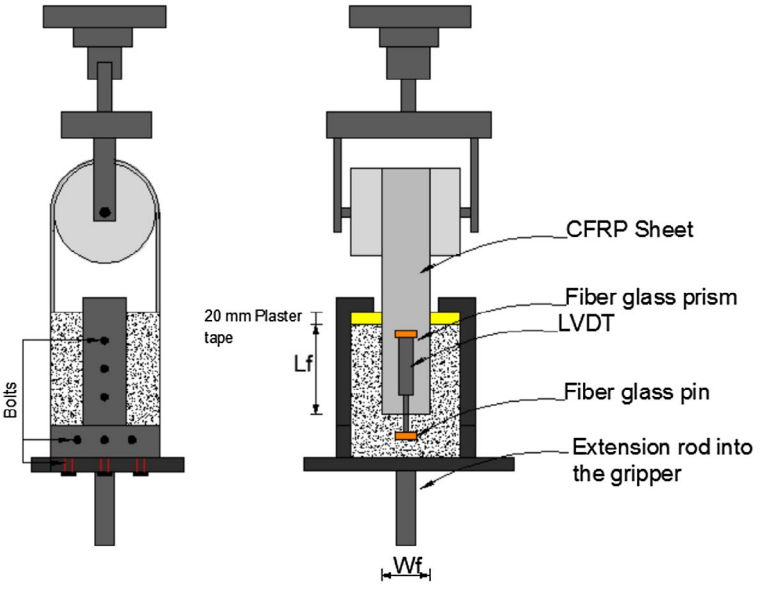

Figure 3. Configuration of test setup used.

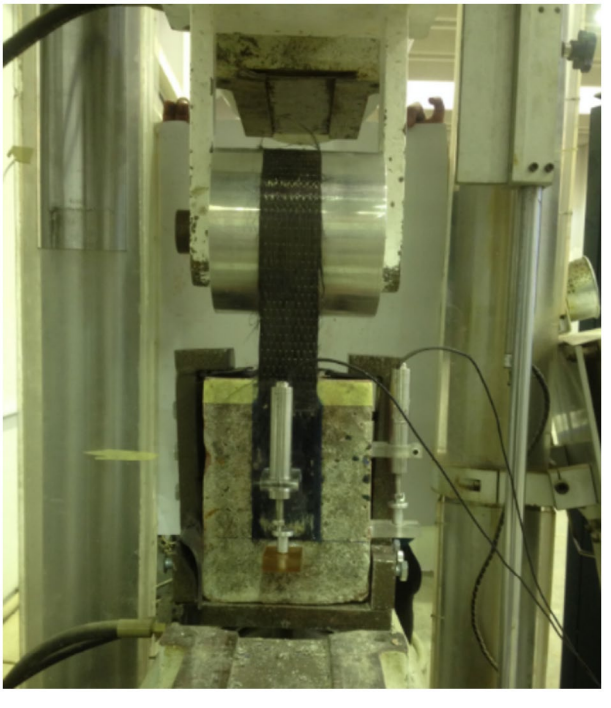

Figure 4. Modified pullout test setup used in present work.

top of the sheet. The specimens were left in laboratory air for a week to allow the adhesive to develop its ultimate adhesion strength.

4.5. Test setup

The bond stress-slip behavior was determined using a near-end pull –off test setup, shown in Figure 3. The pull-off force is applied by a universal testing machine through a U-shaped steel arm pinned to an aluminum cylinder at a loading rate of 0.20 kN/s. As shown, the CFRP sheet raps the aluminum cylinder which is pulled through the U-shaped arm to cause shear failure between the CFRP laminates and the concrete block fixed to the bottom part of the machine, using a special fasteners shown in Figure 4. A Linear Variable Differential Transducers (LVDT) was mounted on the side of concrete blocks where steel reinforcement was positioned. The LVDT was fixed to a prismatic piece of fiber glass pre-glued above the CFRP sheet, while its node was in contact with another prismatic piece of fiber glass, pre-glued to concrete. The load vs. slip readings were acquired using a special data acquisition system. It is important to indicate that as the CFRP sheets were being pulled-off, the concrete substrate underneath was being subjected to tensile stresses; simulating the actual stress condition in repaired flexural members.

5. Results and discussion

The results of the experimental study, carried out to evaluate the effect of reinforcement corrosion cracking on the bond behavior between CFRP sheets and concrete specimens, are presented and discussed in this section. The effect of reinforcement corrosion on cracking pattern and size in corroded concrete blocks is reported and discussed in Section 5.1. Section 5.2. evaluates the extent of damage due to steel corrosion using three non-destructive techniques. The impact of cracking stage on the bond stress-slip diagrams and its characteristics are reported in Section 5.3. with emphasis upon the effect of CFRP sheets' geometric characteristics. The bond failure modes for different specimens are presented

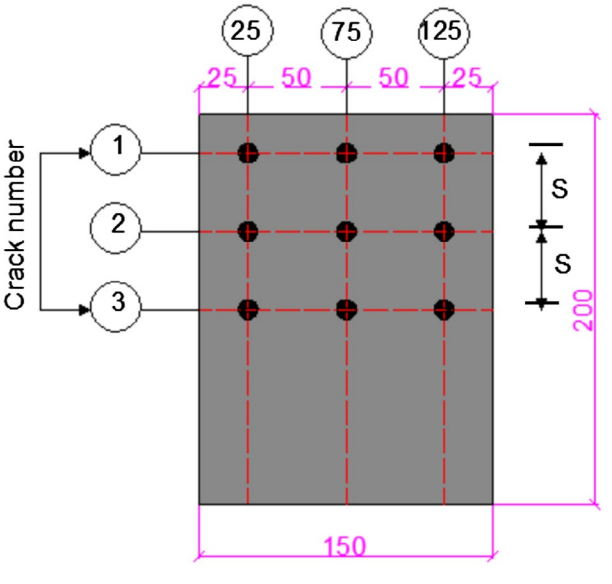

Figure 5. Schematic showing the locations of crack width measurements on the surface of steel corroded blocks (units in mm).

and discussed in Section 5.4. Finally, statistical correlation between different damage indices and residual bond strength between corrosion-damaged concrete and CFRP sheets is presented in Section 5.5.

5.1. Corrosion-induced cracks

Figure 5 shows cracking patterns for the concrete specimens exposed to different corrosion stages. Inspection of pictures revealed that lateral cracks initiated and propagated parallel to some of or all of reinforcement bars. The width of corrosion cracks reached as high as 0.25, 0.64, and 1.1 mm after corrosion stages one, two and three, respectively. The pictures showed also that the number of cracks, parallel to the reinforcement bars, varied from two to three cracks; depending upon the spacing between the reinforcing bars, and the corrosion level [20]. When the distance between reinforcing bars is relatively small, widening of one or more cracks would be on the expense of other cracks, which either get smaller in width or close. It has been also stipulated that further chloride treatment for longer periods led to widening of existing cracks or generation of new ones because of the effect of chloride diffusivity [21]. The crack ranges, reported earlier, are caused by the radial pressure generated by corroding bars, as well as, the pressure by the intruding chloride loaded water [22]. This behavior is demonstrated in the present findings, as cracking on concrete blocks having reinforcing steel at a spacing of 30 and 40 mm appeared on two of the bars only after stages one and two; before another crack immerged along the third bar at the final stage. As expected, the blocks at a spacing value of 50 mm showed three cracks above the steel bars regardless of the corrosion stage.

5.2. Evaluation of corrosion-induced damage

5.2.1. Average crack width

Crack widths were measured using an optical microscope with an accuracy of 0.02 mm at six to nine points along the concrete surface, parallel to steel location according to the schematic of Figure 6. The averages crack widths, computed based upon 12 to 18 readings from two concrete blocks of same reinforcement configuration, are listed in Table 3. The results revealed that crack width increased with higher corrosion levels; due to the increase in the pressure of iron hydroxide (rust) formed by the corrosion mechanism. It can be deduced that regardless of difference in spacing between bars in the different specimens the average crack width showed a narrow range of (0.15–0.20) mm for first stage, (0.53–0.64) mm for the second stage, and (0.85–0.96) mm for the last stage of present treatment. Accordingly, the global crack widths, computed regardless of the reinforcement spacing, were 0.18, 0.60, and 0.90 mm, respectively.

5.2.2. Weight loss of corroded bar

The percentage weight loss of corroded steel bars was computed and listed in Table 3. This was done by determining pre and post-corrosion weights of reinforcing bars. The corroded bars were cleaned using a commercial rest removing liquid. The results showed that the global weight loss after first, second, and third stages were 2.4, 3.8, and 5.6%, respectively.

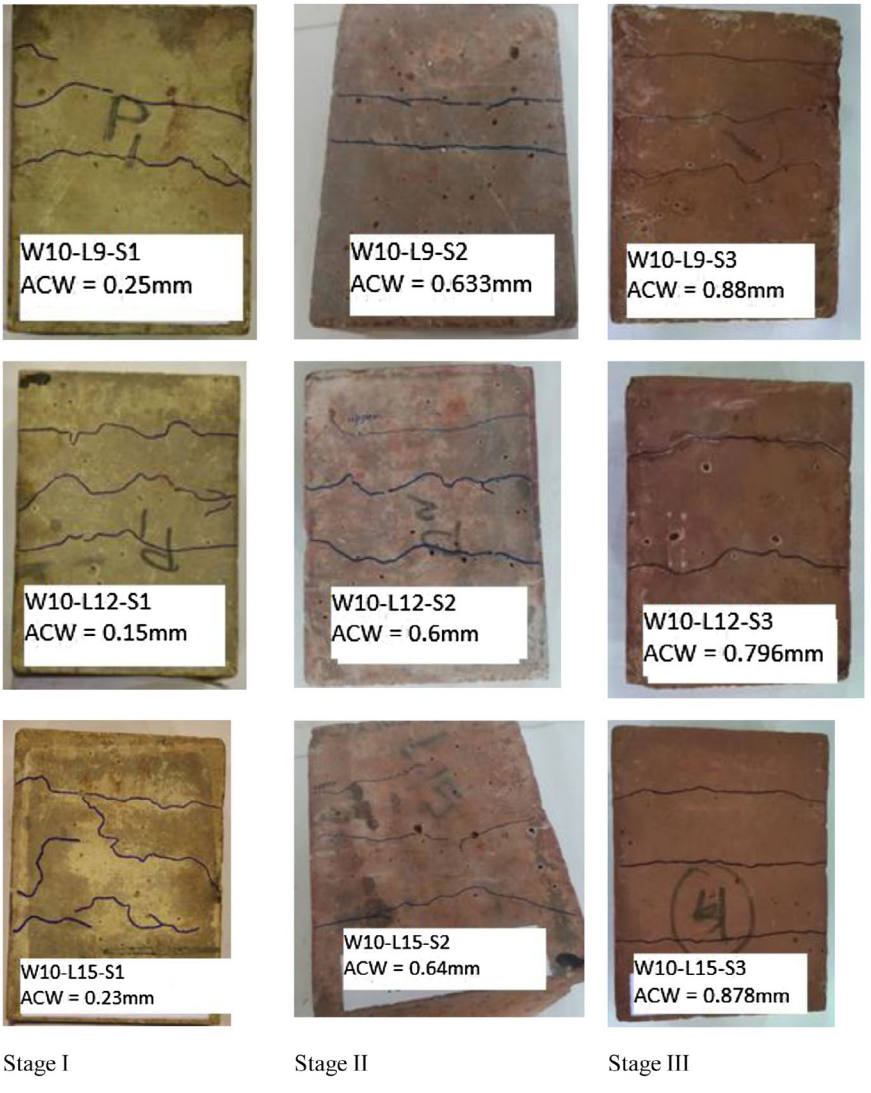

Figure 6. Crack pattern of reinforced concrete blocks prepared with reinforcing steel spaced at 30–50 mm and subjected to three different levels of corrosion treatment.

5.2.3. Ultrasonic pulse velocity

The average ultrasonic pulse velocity (UPV) measurements for intact and corroded concrete specimens were computed upon lag time measured according to ASTM test method C 597 with results listed in Table 3 [16]. Accordingly, a damage index, DI_{UPV}, was computed based upon Equation (1).

$$DI_{UPV} = 1 - \left(\frac{UPV_{Cracked}}{UPV_{Control}}\right)^2 \quad (1)$$

DI_{UPV} is corrosion damage index; and UPV values for intact or cracked concrete.

Results of damage indices in terms of UPV are listed in Table 3. As noticed, the damage indices increased significantly after second and last stages of corrosion; owing to the noticeable increase in cracks width. After first stage, the damage index in terms of the UPV ranged from 7 to 17% yet increased to as high as 24 and 31% after stags two and three, respectively.

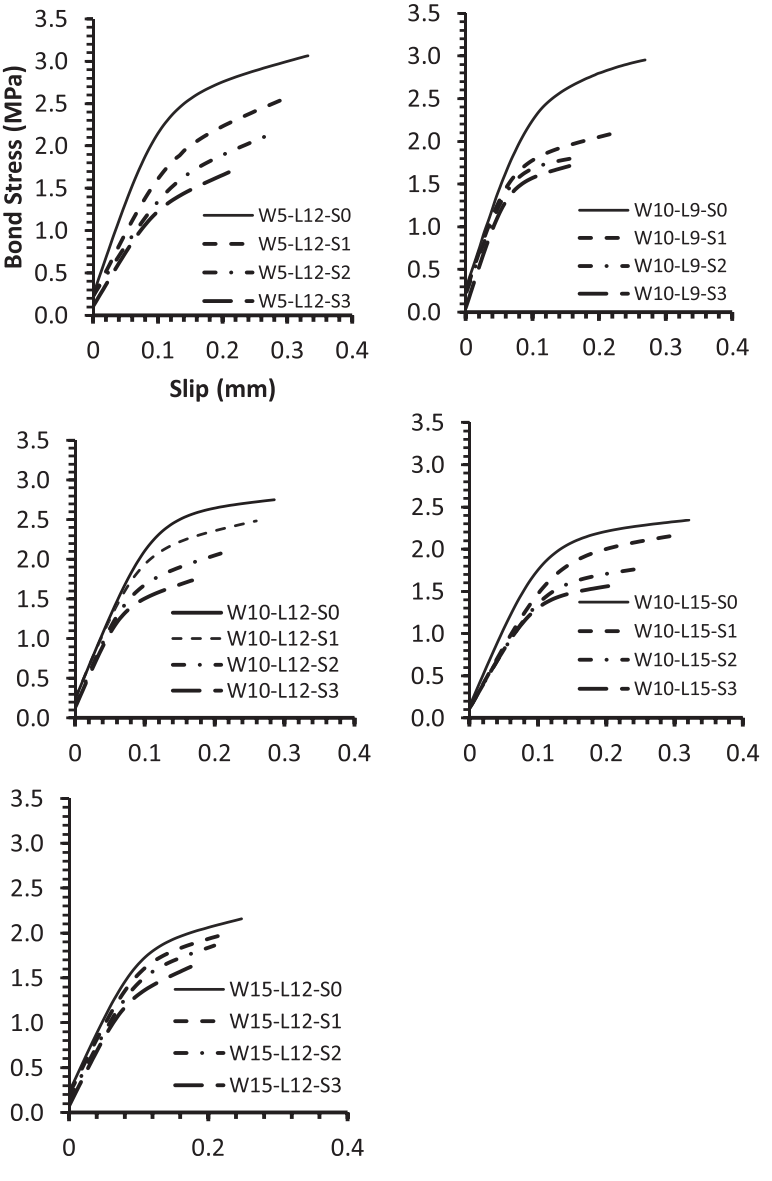

Figure 7. Bond-slip curve for different pull-off specimens after different corrosion levels.

Table 4. Bond characteristics for pull-off specimens with varying corrosion cracking stages.

Specimen designation	CS	UPL (kN)	UBS (MPa)	S_U (mm)	BSS (kPa)	BST (GPa/m)	BT (J/m^2)	FM
W10-L9-S0	NA	26.74	2.97	0.2701	0.279	23.42	600	SP
W10-L9-S1	1	20.10	2.23	0.2255	0.244	22.48	349	SP
W10-L9-S2	2	17.37	1.93	0.1813	0.238	21.42	251	SP
W10-L9-S3	3	15.64	1.74	0.1560	0.049	19.65	195	CCD
W10-L12-S0	NA	33.93	2.83	0.2917	0.254	21.01	618	SP
W10-L12-S1	1	30.35	2.53	0.2603	0.247	20.05	488	SP
W10-L12-S2	2	26.19	2.18	0.2172	0.149	19.69	345	SP
W10-L12-S3	3	21.50	1.83	0.1635	0.133	19.96	211	CCD
W10-L15-S0	NA	37.24	2.48	0.324	0.152	18.39	589	SP
W10-L15-S1	1	32.98	2.20	0.3023	0.128	14.50	497	SP
W10-L15-S2	2	27.00	1.80	0.2413	0.127	13.59	329	SP
W10-L15-S3	3	23.75	1.58	0.213	0.125	13.24	246	SP
W5-L12-S0	NA	18.78	3.10	0.3374	0.259	21.38	771	SP
W5-L12-S1	1	15.85	2.64	0.3067	0.233	14.52	558	SP
W5-L12-S2	2	13.09	2.18	0.2751	0.232	13.82	384	SP
W5-L12-S3	3	10.47	1.75	0.2201	0.112	12.80	245	SP
W15-L12-S0	NA	40.35	2.24	0.2543	0.2327	16.28	399	SP
W15-L12-S1	1	37.82	2.10	0.2243	0.2231	15.11	333	SP
W15-L12-S2	2	33.88	1.88	0.2093	0.1381	14.75	273	CCD
W15-L12-S3	3	30.26	1.68	0.1779	0.0739	14.63	192	CCD

Notes: NA, Not applicable; CS, Corrosion cracking stage; UPL, Ultimate pull-off load; UBS, Ultimate bond strength; S_U, Slippage at ultimate stress; BSS, Bond stress at slippage; BST, Bond stiffness; BT, Bond toughness; FM, Failure mode; SP, Skin peeling-off; CCD, Concrete cover detachment.

Table 5. Residual bond characteristics for pull-off specimens with varying corrosion cracking stages.

Specimen designation	CS	UPL (kN) (%)	UBS (MPa) (%)	S_U (mm) (%)	BSS_0 (kPa) (%)	BST (GPa/m) (%)	Toughness (J/m^2) (%)
W10-L9-S0	NA	100	100	100	100	100	100
W10-L9-S1	1	75	75	83	87	96	58
W10-L9-S2	2	65	65	67	85	91	42
W10-L9-S3	3	58	59	58	17	84	33
W10-L12-S0	NA	100	100	100	100	100	100
W10-L12-S1	1	89	89	89	97	95	79
W10-L12-S2	2	77	77	74	59	94	56
W10-L12-S3	3	63	65	56	52	95	34
W10-L15-S0	NA	100	100	100	100	100	100
W10-L15-S1	1	84	79	84	93	89	89
W10-L15-S2	2	56	74	84	74	73	73
W10-L15-S3	3	42	72	82	66	64	64
W5-L12-S0	NA	100	100	100	100	100	100
W5-L12-S1	1	72	68	90	91%	85	84
W5-L12-S2	2	50	65	90	82	70	70
W5-L12-S3	3	32	60	43	65	56	56
W15-L12-S0	NA	100	100	100	100	100	100
W15-L12-S1	1	83	93	96	88	94	94
W15-L12-S2	2	68	91	59	82	84	84
W15-L12-S3	3	48	90	32	70	75	75

Notes: NA, Not applicable; CS, Corrosion cracking stage; UPL, Ultimate pull-off load; UBS, Ultimate bond strength; S_U, Slippage at ultimate stress; BSS, Bond stress at slippage; BST, Bond stiffness; BT, Bond toughness.

5.3. CFRP-concrete bond

The impact of corrosion on bond behavior between corrosion cracked concrete and CFRP sheet is studied considering the effect of corrosion stage in conjunction with the geometric properties of CFRP sheets.

5.3.1. Effect of corrosion cracking

The effect of different corrosion stages on the bond behavior between CFRP sheets and concrete can be understood from Figure 7. As shown, the different curves followed a common trend represented in linear up to 50% of ultimate bond stress followed by a nonlinear behavior afterwards. At higher corrosion stages, the ultimate bond strength showed a significant decrease, while slip at failure following a common decreasing trend; owing to further deterioration in concrete due to steel corrosion. The characteristics of the different bond stress-slip curves, namely ultimate bond stress, ultimate slippage, bond stress at slippage, bond stiffness and bond toughness were computed and are listed in Table 4.

The results of Table 4 indicate clearly that the characteristics of bond stress versus slip relationship were decreased because of the occurrence of corrosion cracking at perpendicular orientations to that of CFRP fibers. The relevant residuals of Table 5 were decreased with corrosion cracking extent with reduction percentages being dependent upon the test specimens' geometric properties. The residual bond strength of corrosion cracked pull-off specimens ranged from 59 to 93%, whereas the slippage at ultimate stress ranged from 32 to as high as 96%, respectively. The bond stress at slippage was slightly reduced by corrosion after the first two stages, yet significantly reduced after the final stage of corrosion with residuals of (17 to 70%). On contrast, the bond stiffness was affected by the corrosion cracks the least with residuals ranging from (56 to 95%) after the final corrosion stage considered in this work. Finally, the bond toughness showed the highest sensitivity toward corrosion cracking, as residuals were reduced to as high as 58, 42, and 33% after first, second, and final stages of corrosion treatment, respectively.

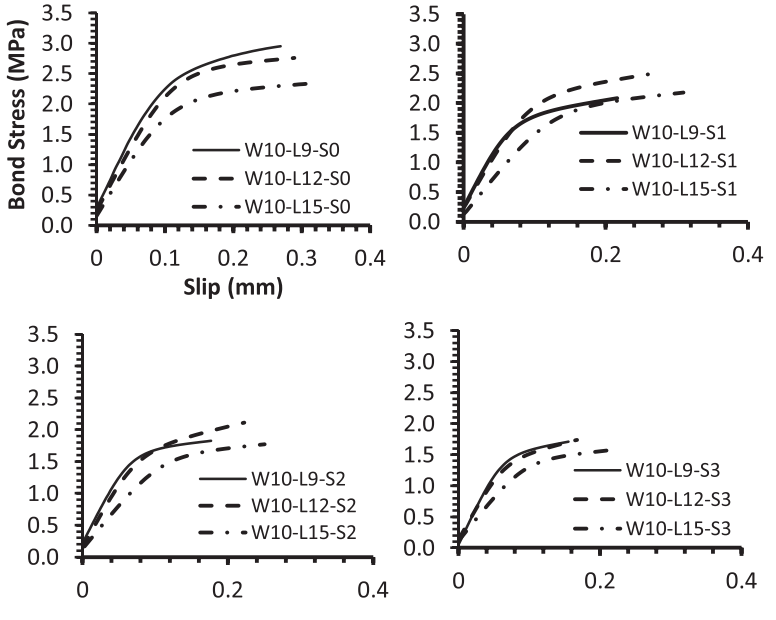

Figure 8. Effect of bond length upon bond-slip relationship for pull-off specimens with different steel corrosion cracking levels.

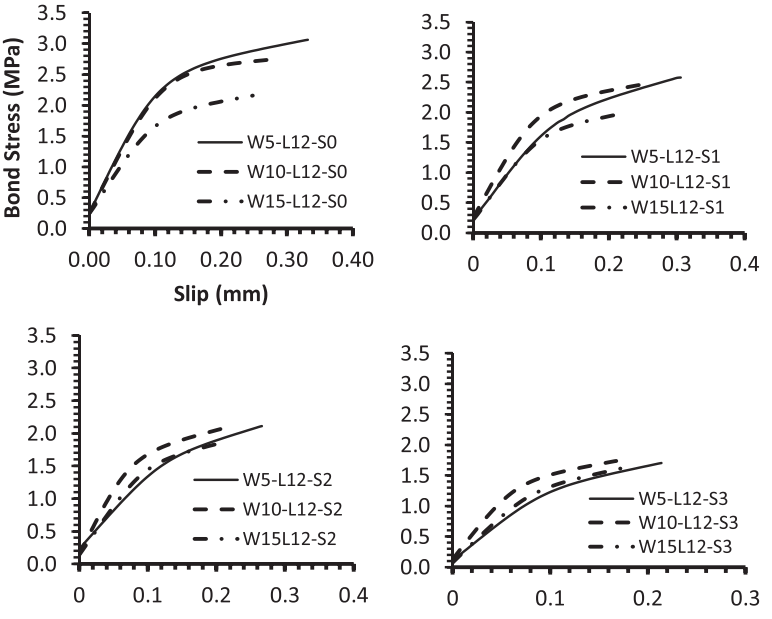

Figure 9. Effect of bond width upon bond-slip relationship for pull-off specimens with different steel corrosion cracking levels.

5.3.2. Effect of CFRP geometry

The bond characteristics of Figure 8 through 9, namely bond strength and stiffness, pertaining to control (undamaged) pull-off specimens were reduced whereas ultimate bond slippage increased with bond lengths ranging from 90 to 150 mm. On contrast, the same bond characteristics were reduced when CFRP sheets were bonded to the undamaged concrete blocks at large bond width in the range of 50–150 mm.

Exposure of various pull-off specimens to corrosion resulted in residual properties of varying magnitudes depending upon the geometric properties of CFRP (bond length and width) with minimal values at the final stage. Figure 8 showed that the pull-off specimens at the lowest bond length were the most susceptible to corrosion cracking; showing the lowest residual properties, followed in sequence by those at bond lengths of 120 and 150 mm. The results showed that the differences between the residual characteristics of pull-off specimens at different bond lengths tended to decrease as corrosion progressed; especially for the cases where bond failure became dictated by concrete cover peeling-off. This may not be true regarding bond stress at slippage which showed higher susceptibility to corrosion cracking in pull-off specimens at the lower bond length. The results also demonstrated that bond toughness was the least affected by corrosion cracks; especially for the cases where bond failure was caused by concrete skin peeling-off. The residual characteristics (ultimate bond stress, slippage at ultimate stress, bond stress at slippage, bond stiffness, and bond toughness) for pull-off specimens at bond lengths of 90, 120, and 150 mm after first stage were (75, 83, 87, 96, and 58%), (89, 89, 97, 95, and 79%), and (79, 84, 93, 89, and 89%), whereas the corresponding residuals after the last stage were (59, 58, 17, 84, and 33%), (65, 56, 52, 95, and 34%), and (72, 82, 66, 64, and 64%), respectively.

Figure 9 indicated that except for slippage at ultimate stress, other bond characteristics showed higher susceptibility to corrosion cracks for pull-off specimens having CFRP sheets' bond width of 50 and 100 mm than at 150 mm. The residuals for (ultimate bond stress, slippage at ultimate stress, bond stress at slippage, bond stiffness, and bond toughness) after first stage were (68, 90, 91, 85, and 84%), (89, 89, 97, 95, and 79%), and (93, 96, 88, 94, and 94%) for pull-off specimens at bond widths of 50, 100, and 150 mm respectively. The corresponding residuals after the last stage were (60, 43, 65, 56, and 56%), (65, 56, 52, 95, 34%), and (90, 32, 70, 75, and 75%), respectively.

The distribution stipulated for shearing stress and shown in Figure 1 suggests that the average bond stress would be lower for control specimens with longer bond lengths

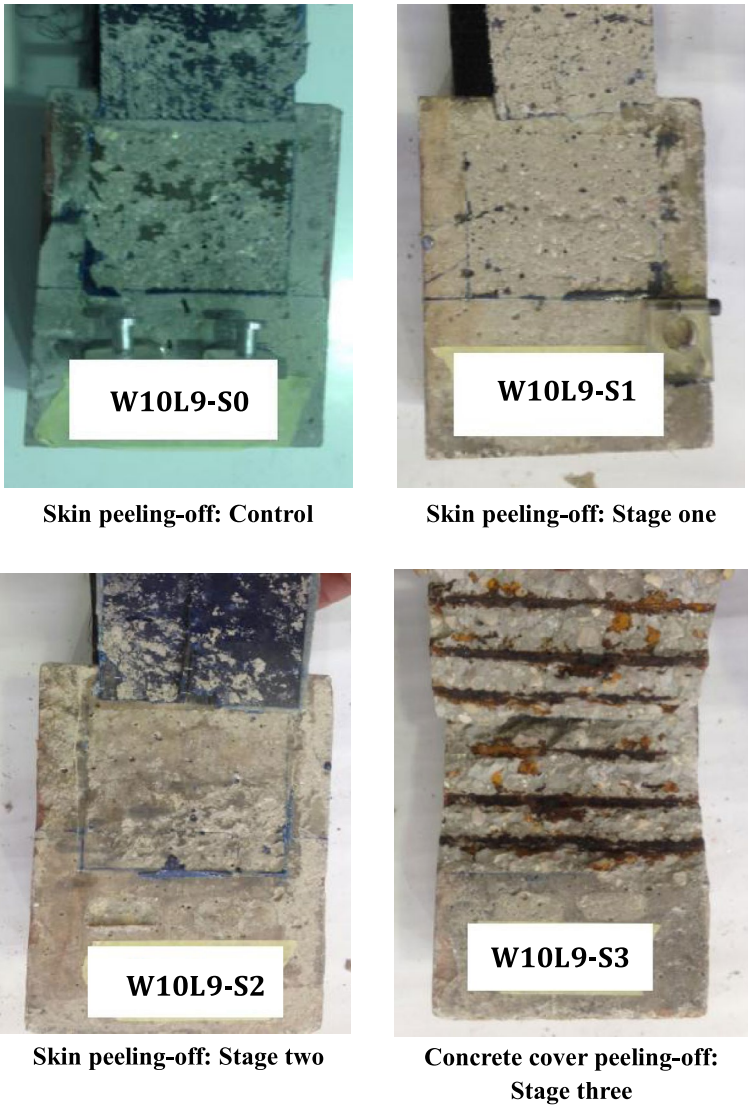

Figure 10. Failure modes for W10L9 pull-off specimens at different stages of corrosion cracking.

because of the increased deviation between maximum and minimum shearing stresses [23]. Logically, lower slippage at ultimate stress is expected for specimens with higher bond length and vice versa. Based on this argument, pull-off specimens with lower bond length would be more determinately affected by corrosion cracks as the deviation between maximum and minimum shearing stresses is lower, hence the average bond stress would be increased which results in faster propagation and widening of pre-existing cracks. This would not be true when bond failure mode is caused by concrete cover detachment as cracks' effect on bond between CFRP and concrete would be negligible.

The higher bond strength for control pull-off specimens at the lower bond widths is related to the limited variation in shearing stress across width, as indicated by Figure 1. The higher degradation in bond characteristics in the pull-off specimens at the lower bond width, upon formation of corrosion cracks, is related to the inability of the CFRP sheet, rather thin in width, to arrest and/or control the opening of the already existing corrosion

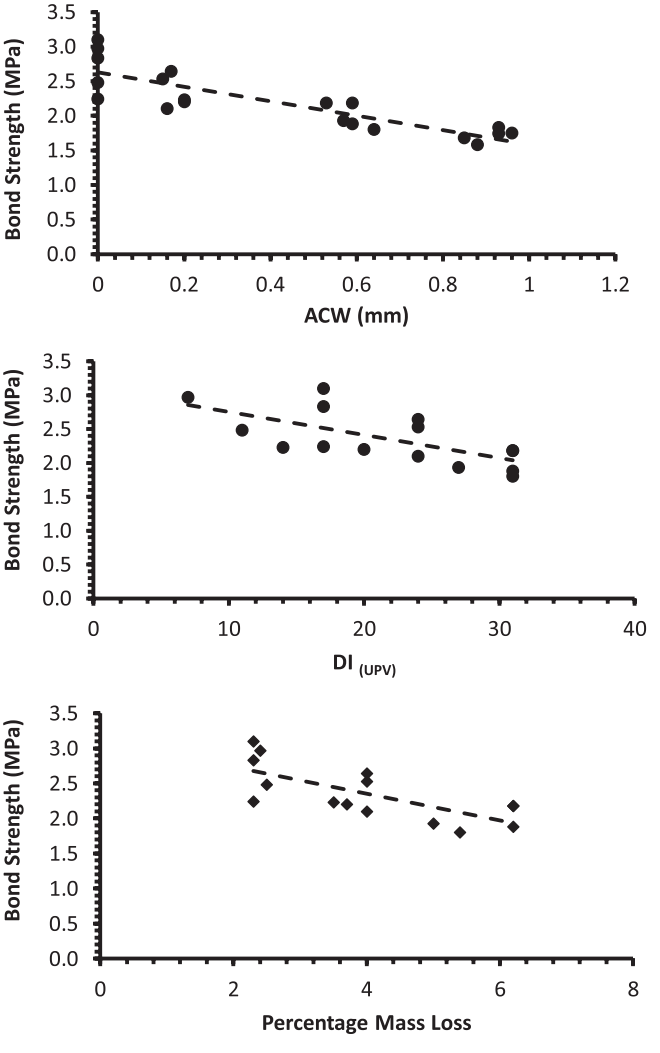

Figure 11. Damage indices in terms of ACW, UPV, and Mass loss vs. bond strength.

Table 6. Bond strength regression models.

Variables			
Dependent	Independent	Equation	R^2
UBS	ACW	UBS = −1.045ACW + 2.629	0.740
UBS	DI_{UPV}	UBS = −0.0341DI_{UPV} + 3.049	0.453
UBS	ML	UBS = −0.190ML + 3.114	0.520

Note: UBS, Ultimate bond stress; UPV, Ultrasonic pulse velocity; DI_{UPV}, Damage index in terms of UPV; ML, Mass loss (%).

cracks. This argument stands true as long as bond failure is caused by concrete skin peeling-off rather concrete cover detachment.

5.4. Bond failure modes

During the first few seconds of the pull-off test procedure, the specimens showed no signs of debonding. The test setup used for pull-off test allowed concrete in contact with CFRP sheets to elongate as the universal testing machine head was displaced further which caused the already existing corrosion cracks that varied in number across the bond length from 2 to 3 to widen further; leading ultimately to bond failure, accompanied with loud failure sound. Of course, the time to failure was shorter for specimens with higher average cracking width; owning to the increased impact of stress concentration on CFRP detachment from concrete.

For some blocks, concrete cover was detached at failure; owing to the extension of cracks at steel bars level in a direction parallel to the fiber direction via CFRP sheets. Hence, two failure modes were identified; either concrete skin peeling-off or detachment of concrete cover. Figure 10 show typical failure patterns for pull-off specimens having similar steel bar spacing yet underwent different corrosion extents. The failure modes were dependent upon geometric characteristics of CFRP sheets and corrosion levels, as summarized in Table 4. Failure mode occurred through skin peeling-off failure for control specimens and those subjected to first corrosion stage; regardless of bond length or width of CFRP sheets, yet changed to concrete cover peeling-off for specimens at bond widths of 100 and 150 mm and lengths of 90 and 120 mm (bar spacing of 30 and 40 mm) after either stages two or three of corrosion cracking.

5.5. Correlating residual bond strength to damage indices

Regression models have been developed to relate bond strength to average crack width, as shown in Figure 11(a). The model equations of Table 6 showed that bond strength is significantly affected by increasing average crack width. The regression results indicated a reasonable coefficient of determination (R^2) at 0.74.

The correlations between bond strength and damage indices in term of UPV, and percentage mass loss is illustrated in Figure 11(b) and (c), respectively. The models reflected negative impact of increasing damage indices in terms of UPV and percent loss in steel weight. The corresponding correlation equations were obtained and are listed in Table 6. As notice, a mild correlation can be identified at R^2 values of around 0.5. The correlation between different damage indices and slip at ultimate stress was poor; hence corresponding empirical models were not reported.

6. Conclusions

The following points highlight the main outcomes and conclusions extracted from the test results:

(1) The cracks observed on the surface of concrete blocks were parallel to the reinforcement bars and varied from two to three cracks depending upon the spacing between the reinforcing bars, and the corrosion level. The width of cracks increased with corrosion stages reaching a maximum of 1.1 mm after the last stage.
(2) The global mass loss of steel reinforcement due to corrosion increased from 2.4% at first to 5.6% at the final stage.
(3) The bond stress-slip relationship of various pull-off specimens maintained the same curve shape, regardless of the CFRP sheets' geometric characteristics or corrosion cracking extent. It showed linear behavior after imitation of slippage until a point representing about 50% of ultimate bond stress before became nonlinear until failure.
(4) The reinforcement corrosion reduced bond characterizes, namely, bond strength, bond stress at slippage, ultimate slippage, bond stiffness and bond toughness between CFRP sheets and concrete with corroding steel by as much as 41, 83, 68, 44, and 67%, respectively.
(5) The impact of corrosion cracks was more detrimental as bond length and width was decreased; especially at first and second corrosion stages. After the third stage, the magnitude of reduction in bond characteristics was either unaffected or slightly affected by CFRP sheet's geometric properties.
(6) The failure mode for pull-off specimens, having reinforcing steel bars spacing of 30–40 mm (corresponding sheets' bond length of 90 and 120 mm), changed from skin peeling-off to concrete cover detachment at the last stage.

It is important to mention that cracking spacing to bond length ratio was kept constant at 1/3 in present pull-off specimens. Hence, it is recommended to carry out future testing to establish the impact of this factor on bond behavior between cracked concrete and CFRP sheets, leading to the development of analytical models to describe bond behavior in cracked and repaired concrete elements.

Acknowledgement

The authors acknowledge the technical and financial support provided by the research deanship at Jordan University of Science and Technology and the assistant by the technicians at the structural and materials laboratory via the Department of Civil Engineering.

Disclosure statement

No potential conflict of interest was reported by the authors.

Funding

This work was supported by the research deanship at Jordan University of Science and Technology [project number 172/2015].

References

[1] Neville AM. Properties of concrete. 4th and final ed. Essex: Addison Wesley Longman Limited; 1995.
[2] Sun J, Huang Q, Ren Y. Performance deterioration of corroded RC beams and reinforcing bars under repeated loading. Constr Build Mater. 2015;96:404–415.
[3] Yu L, Francois R, Dang VH, et al. Distribution of corrosion and petting factor of steel in corroded RC beams. Constr Build Mater. 2015;95:384–392.
[4] Song L, Yu Z. Fatigue performance of corroded reinforced concrete beams strengthened with CFRP sheets. Constr Build Mater. 2015;90:99–109.
[5] Almassri B, Kreit A, Al Mahmoud F, et al. Behavior of corroded shear-critical concrete beams repaired with NSM CFRP rods. Compos Struct. 2015;123:204–215.
[6] Azam R, Soudki K. Structural performance of shear-critical RC deep beams with corroded longitudinal steel reinforcement. Cem Concr Compos. 2013;23:946–957.
[7] Jones R, Swamy RN, Charif A. Plate separation and anchorage of reinforced concrete beams strengthened by epoxy-bonded steel plates. Struct Eng. 1988;66(5):85–94.
[8] Hussain M, Sharif A, Basunul IA, et al. Flexural behavior of precracked reinforced concrete beams strengthened externally by steel plates. Struct J. 1995;92(1):14–22.
[9] Haddad RH, Shannag MJ, Al-Hambouth MT. Repair of reinforced concrete beams damaged by alkali-silica reaction. ACI Struct J. 2008;105(2):145–153.
[10] Haddad RH, Shannag MJ, Moh's A. Repair of heat-damaged shallow beams using advanced campsites. Mater Struct. 2008;41:287–299.
[11] Al-Rousan R, Haddad R, Al-Sa'di K. Effect of sulfates on bond behavior between carbon fiber reinforced polymer sheets and concrete. Mater Des. 2013;43:237–248.
[12] Haddad R, Al-Rousan R, Almasry A. Bond-slip behavior between carbon fiber reinforced polymer sheets and heat-damaged concrete. Compos Part B. 2013;45(1):1049–1060.
[13] Haddad R, Al-Rousan R. An anchorage system for CFRP strips bonded to thermally shocked concrete. Int J Adhes Adhes. 2016;71:10–22.
[14] Siad A, Bencheikh M, Hussein L. Effect of combined pre-cracking and corrosion on the method of repair of concrete beams. Constr Build Mater. 2017;132:462–469.
[15] Osman BH, Wu E, Bohai J, et al. Repair technique of pre-cracked reinforced concrete (RC) beams with transverse openings strengthened with steel plate under sustained load. J Adhes Sci Technol. 2017;31(21):2360–2379.
[16] Aiello M, Focacci F, Huang PC, et al. Cracking of concrete cover in FRP reinforced concrete elements under thermal loads. In: Dolan CW, Rizkalla SH, Nanni A, editor. Proceeding of the 4th International Symposium on FRP for Reinforcement of Concrete Structures (FRPRCS4); Baltimore, MD; 1999.
[17] Subramaniam KV, Ghosn M, Ali-Ahmad M. Influence of variation in the local interface fracture properties on shear debonding of CFRP composite from concrete. J Adhes Sci Technol. 2017;31(19–20):2202–2218.
[18] ASTM Specification. American society for testing and materials international. West Conshohocken, PA: ASTM International; 2004.
[19] ACI Manual of Concrete Practice. Standard practice for selecting proportions for normal, heavyweight, and mass concrete (ACI 211.1), Part I: Materials and General Properties of Concrete. Detroit, MI; 2008.
[20] Shi X, Yang Z, Liu Y, et al. Strength and corrosion properties of Portland cement mortar and concrete with mineral admixtures. Constr Build Mater. 2011;25:3245–3256.
[21] Wang HL, Dai JG, Sun XY, et al. Characteristics of concrete cracks and their influence on chloride penetration. Constr Build Mater. 2016;107:216–225.
[22] Bassuoni MT, Rahman MM. Response of concrete to accelerated physical salt attack exposure. Cem Concr Res. 2016;79:395–408.
[23] Subramaniam KV, Carloni C, Nobile L. Width effect in the interface fracture during shear debonding of FRP sheets from concrete. Eng Fract Mech. 2007;74:578–594.